











Transverse emittance growth of proton sources from laser-irradiated sub- μm -thin planar targets

Thomas F. Rösch ^{1,*}, Masoud Afshari ^{1,†}, Felix Balling ¹, Leonard Doyle ¹, Sonja Gerlach ¹, Jens Hartmann ¹,
Alexander Prasselsperger ¹, Stuart Morris ² and Jörg Schreiber ^{1,‡}

¹Fakultät für Physik, Ludwig-Maximilians-Universität München, 85748 Garching, Germany

²Department of Physics, University of Warwick, Coventry CV4 7AL, United Kingdom

 (Received 11 April 2023; revised 7 August 2023; accepted 13 December 2023; published 2 February 2024)

Proton bunches with maximum energies between 12 and 22 MeV were emitted from submicrometer-thin plastic foils upon irradiation by laser pulses with peak intensity of $4 \times 10^{20} \text{ W/cm}^2$. The images of the protons by a magnetic quadrupole doublet on a screen remained consistently larger by a factor of 10 compared to expectations drawn from the ultralow transverse emittance values reported for thick foil targets. Analytic estimates and particle-in-cell simulations attribute this drastically increased emittance to formerly excluded Coulomb collisions between charged particles. The presence of carbon ions and significant transparency likely play a decisive role. This observation is highly relevant because such thin, partially transparent foils are considered ideal for optimizing maximum proton energies.

DOI: [10.1103/PhysRevE.109.025201](https://doi.org/10.1103/PhysRevE.109.025201)

I. INTRODUCTION

Laser-driven ion sources hold promise for a number of applications [1], in particular when extremely high peak particle fluences are required. Acceleration typically happens in a plasma, where a highly intense laser pulse creates relativistic electrons that penetrate the thin target foil and set up strong charge separation fields at the plasma-vacuum interfaces. Electrons remain bound to the target and form a sheath in which protons [2] and heavier ions [3] are accelerated via target normal sheath acceleration (TNSA). One of the particular properties of a TNSA proton bunch is the ultrasmall transverse bunch emittance,

$$\varepsilon_x = (\sigma_x^2 \sigma_{x'}^2 - \sigma_{xx'}^2)^{1/2}, \quad (1)$$

a phase space quantity that relates the bunch width σ_x with the divergence $\sigma_{x'}$ in direction x under consideration of the correlation between these quantities $\sigma_{xx'}$ [4]. The same holds independently for the orthogonal transverse dimension y . These bunch properties relate to the bunch phase space $f(x, x')$ according to $\sigma_x^2 = \iint x^2 f(x, x') dx dx'$, $\sigma_{x'}^2 = \iint x'^2 f(x, x') dx dx'$ and $\sigma_{xx'} = \iint xx' f(x, x') dx dx'$, where x is a single particle's position and x' is the particle's angle with respect to the main trajectory, in case of this work the optical axis of a magnetic quadrupole doublet. A small emittance results in a high laminarity of the bunch and enables good focusability. In concert with the large number of particles contained in one bunch, this promises very high proton fluences and new approaches to experiments, for example in material science and nuclear physics.

Various approaches based on, e.g., structured targets [5] or metallic meshes [6] have been employed for determining the emittance of sources from micrometer thick foils, where the TNSA mechanism was the dominating acceleration mechanism. It was concluded that the small emittance was a result of the relatively cold, unperturbed target rear surface that allows for a laminar and sudden acceleration with small transverse momentum spread. Most prominent is the upper limit value published by Cowan *et al.* [5], where a target with microgrooves on the rear side served for estimating the normalized transverse bunch emittance of 10-MeV protons from 18- μm aluminum foils to $<0.004 \text{ mm mrad}$.

Although the TNSA mechanism with rather thick targets is robust, it scales only modestly with laser intensity [7–9]. Therefore, many groups have dedicated effort in improving the temporal contrast to minimize premature plasma expansion. This allowed exploring acceleration mechanisms with more favorable scaling than TNSA. In this quest, reducing the thickness of foil targets from several micrometers to 1 μm and below has recently proven beneficial for achieving higher ion energies [10–14]. Beyond TNSA, the volumetric interaction of the laser with the plasma due to induced transparency [15] seems to play a decisive role. To the best of our knowledge, no measurement of the emittance of these thin partially transparent foil targets was reported, likely because manufacturing of structures on the rear side is challenging for very thin foils, in particular because they are typically made out of plastic. The pepper-pot method based on a mesh behind the target is prone to disturbances, for example due to the interaction with energetic electrons or the partially transmitted intense laser light that can affect the proton phase space postacceleration [16]. We therefore attempted determining the transverse emittance of protons emitted from laser-irradiated sub- μm -thin plastic foils by analyzing the smallest spots that we could create with a magnetic quadrupole doublet, similar to the established quadrupole scanning method [4]. We use only two

*t.roesch@physik.lmu.de

†m.afshari@physik.lmu.de

‡joerg.schreiber@lmu.de

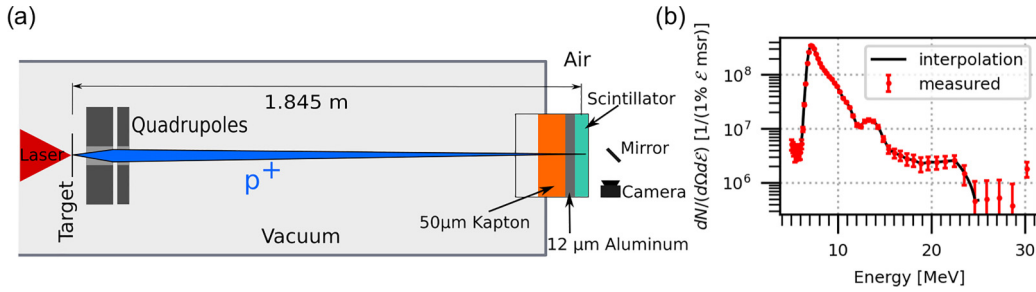


FIG. 1. (a) Experiment setup. Protons accelerated from a sub- μm -thin foil are focused by a pair of permanent magnet quadrupoles onto a scintillator outside the vacuum chamber. (b) Differential energy distribution of protons measured with magnetic spectrometer without quadrupoles in vacuum.

measurement planes, the proton focal plane where the spot has minimal size and the quadrupole entrance aperture, where the beam is significantly larger than the source and focus.

II. PROTON FOCUS ANALYSIS

A. Experimental setup

The advanced Ti:Sa laser system ATLAS at the Centre for Advanced Laser Applications (CALA) provided laser pulses with a full width at half maximum (FWHM) duration of about 28 fs. At the experimental area for laser-ion acceleration (LION), the pulses were focused by a $f/5$ 20° off axis parabolic mirror yielding a peak intensity of about 4×10^{20} W/cm², corresponding to a normalized vector amplitude of 14, in a focus with FWHM diameter of 4.6 μm . Plastic foils with thicknesses of 400 and 600 nm served as targets and were irradiated under an angle of 6.8° with respect to the laser direction. These foil thicknesses had been identified to provide reliable proton emission within a broad energy distribution that extended to maximum energies of up to 25 MeV [Fig. 1(b)]. The proton emission was accompanied by transmission of laser energy between 0.01 and 0.1%.

A pair of permanent magnet quadrupoles refocused a narrow energy range around a selected energy; we refer to this as focused energy, 1.845 m downstream of the target onto a scintillator that was imaged with 15 μm spatial resolution. As indicated in Fig. 1(a), the scintillator was mounted on air in direct contact to a vacuum exit window made out of 50- μm -thick kapton and 12 μm aluminum. It is important to clarify that the focused energy is a nominal value that relates to the drift lengths between the quadrupoles. The real particle energy in the focus is slightly lower due to the energy loss in the exit window. The actual spectrum of the protons within the focal spot is peaked at this energy with a relative energy spread of a few %. Each quadrupole consisted of 12 wedges of NdFeB magnets arranged in a Halbach design [17] with a bore aperture of 10 mm and a total diameter of 50 mm. The lengths of the first and second magnets were 40 and 20 mm, whose effective gradients, estimated with three dimensional Hall probe measurements, were (332 ± 13) and (334 ± 13) T/m, respectively. Both quadrupoles (QPs) had been tested at a 20-MeV proton beam from a tandem Van de Graaff accelerator, and in combination they proved capable of producing a focal spot with diameter smaller than our detector resolution of 50 μm . Given the total length of 176 mm from the QP doublet entrance to the focus, these preceding studies

suggested that geometrical emittances $\gtrsim 0.5/176$ rad \times 25 $\mu\text{m} \approx 0.1$ mm mrad could be reliably measured.

For the laser-ion experiment, the doublet was set up in a way that the first magnet was focusing in vertical and defocusing in the horizontal dimension and the second quadrupole vice versa, giving a focusing-defocusing (FODO) configuration in vertical and defocusing-focusing (DOFO) one in horizontal dimension. The magnets were positioned downstream of the proton source using motorized stages capable of remotely adapting the drift lengths between the magnets and the transverse position of the doublet with a precision of 10 μm , as well as the relative angle with a precision of 1 mrad [18]. The remaining degrees of freedom were manually adjusted. The setup was prealigned using a three-axis Hall probe with an accuracy of 200 μm and 0.1° and optimized on the beamline. The drift lengths were initially set to calculated values for the desired focused energy. The lowest focused energy, 12 MeV, was thereby determined by the shortest possible distance between the target and the first quadrupole. From these starting positions, a variation of the drifts was performed to minimize the spot size on the scintillator. This optimized position resulted in an adjustment of the calculated values by about 1 mm.

B. Measurement results

The background subtracted images yielded information on the FWHM diameter of the spot in the vertical and horizontal dimension. In addition, we calculated the integral of the image as a measure for (relative) particle number. Figure 2(a) shows one typical focus image with the quadrupole setup optimized to focus 12 MeV. The spot is elliptical and has a FWHM diameter of 1.49 ± 0.08 mm in vertical and 0.56 ± 0.05 mm in horizontal dimension. Figure 2(b) shows the diameters of 31 consecutively produced proton foci with the same settings. The proton foci had an average extension of 1.4 and 0.53 mm with a standard deviation of 0.4 (29%) and 0.07 mm (13%), respectively. The integral over the background subtracted scintillator images varies by about one order of magnitude over the 31 shots, but it is not correlated to the beam size. In contrast, the two FWHM diameters in the orthogonal transverse dimensions are correlated. In addition to the study at the QP setting for focusing 12-MeV protons, we have taken data for the optimum setting for focusing protons with 14, 16, 18, 20, and 22 MeV. Figure 2(c) shows the average FWHM diam-

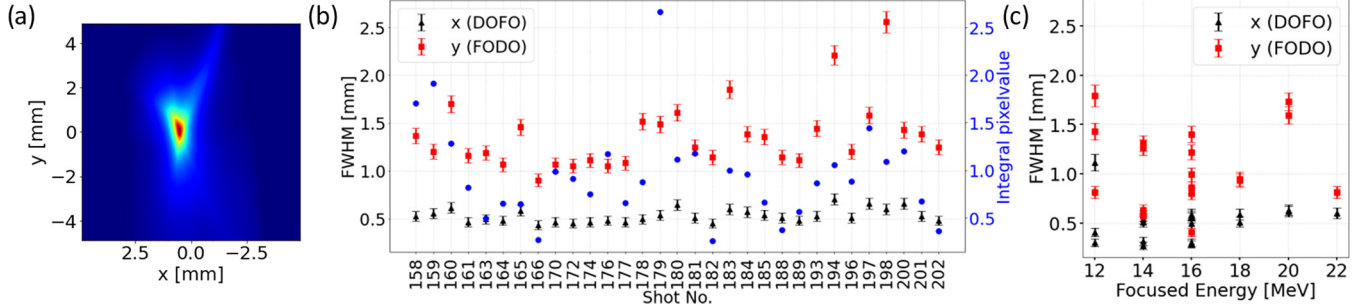


FIG. 2. (a) Exemplary 12-MeV proton focus with optimized focusing geometry. Optimized proton spot size for (b) 12 MeV in 31 consecutive shots and (c) varied focused energy between 12 and 22 MeV.

eters as a function of focused energy. Within the shot-to-shot fluctuations, there is no systematic dependence on energy.

C. Beamline modeling

For interpreting the measured proton spot sizes, the beam line in Fig. 1(a) was modeled using ion optical beam transfer matrices [4] to predict the proton fluence distribution in the focal plane as a function of emittance. The acceptance angles of the setup, defined by the limited aperture of the bore and an additional protection plate in front of the first quadrupole, were 31 and 15 mrad in horizontal and vertical dimension, respectively and much smaller than the typical global divergence angle of laser-accelerated protons. Therefore, we assumed a flat angular distribution truncated by the transport system. As the quadrupole matrices depend on the bunch momentum via the focusing strength, a representative proton spectrum [Fig. 1(b)] was discretized into steps of 2 keV and each energy value was transported through the matrices. The resulting spatial distribution in the focal plane was then weighted by the proton spectral amplitude and integration over proton energy yielded the fluence distribution. The initial transverse phase space of the bunch at the source was represented by assuming an energy independent (and *a priori* unknown) set of bunch parameters for width and divergence in the transverse dimensions, σ_x , $\sigma_{x'}$, σ_y , and $\sigma_{y'}$. We interpreted the beam width obtained from the matrix calculation as the width of a Gaussian distribution in the focal plane. The drift lengths were chosen such as to focus 12-MeV protons, representing the lowest energy investigated in the experiments for which we have recorded the largest data set.

D. Evaluation of emittance

Figure 3 shows the expected fluence distributions for three important cases. First, to determine the lower limit of the expected focal spot size an initial proton bunch of zero emittance was transported through the beamline. Therefore, the bunch was modeled with zero width in the transverse dimensions at the laser target position. Figure 3(a) shows that the focal spot of a point source yields a spot with FWHM diameter of 60 μm in both dimensions. This is a consequence of the broad spectrum of the bunch where the particles with energies other than the focused energy significantly contribute to the fluence distribution. Figure 3(b) shows the expected focus distribution for the normalized transverse emittance of 0.004 mm mrad

measured by Cowan *et al.* [5]. Considering our acceptance angles and the geometrical emittance for 10-MeV protons, this normalized emittance corresponds to a geometrical emittance of 0.03 mm mrad which is represented by a FWHM diameter of the virtual source $\sigma_{x,0} = 2 \mu\text{m}$ and $\sigma_{y,0} = 1 \mu\text{m}$. For this case, the predicted fluence distribution on the scintillator has a FWHM of 60 μm in the x dimension and 180 μm in the y dimension. While the horizontal size is still governed by the spectrum, the larger magnification in the vertical dimension creates an elongated focus that is significantly larger than in the horizontal dimension. Figure 3(c) shows the expected proton focus for a geometrical emittance of 0.3 mm mrad. The proton focus has dimensions 700 μm in x and 1500 μm in y , the asymmetry is similar to the case of small emittance. This shows that the different magnifications in the two orthogonal directions clearly govern the focus shape, as soon as the emittance is larger than zero. Figure 3(d) exemplifies the proton energy distributions that would emerge after a 1-mm-diameter aperture showing that spectral effects for one focused energy are insignificant when the emittance changes.

Figure 3(e) aids the discussion of the results by combining calculated and measured FWHM diameters of proton foci as a function of assumed geometrical emittance of the source. The shaded regions represent the margins of the experimentally determined emittance values. The width of the region was conservatively chosen as the minimal and maximal values observed in the 31 shots for a focused energy of 12 MeV. The pragmatic interpretation of this result is that the geometrical emittance of the transported 12-MeV proton beam is larger than 0.17 and 0.2 mm mrad for the vertical and horizontal dimension, respectively. Even within the sizable margins, this is much larger than is typically quoted for TNSA sources.

III. DISCUSSION OF EXPERIMENTAL RESULTS

Unidentified field errors of the quadrupoles could contribute and lead to misinterpretation of the emittance. The aforementioned prior measurements at a conventional proton beam have revealed that such imperfections can be excluded as long as the estimated emittance is larger than 0.1 mm mrad. Therefore, field errors cannot be excluded but are unlikely to be responsible for the large emittance. In addition, the observation of significant shot-to-shot fluctuations supports the meaningfulness of our measurement. If the proton spot size was limited by imaging resolution or other artefacts, we would not expect to be sensitive to fluctuations of a beam

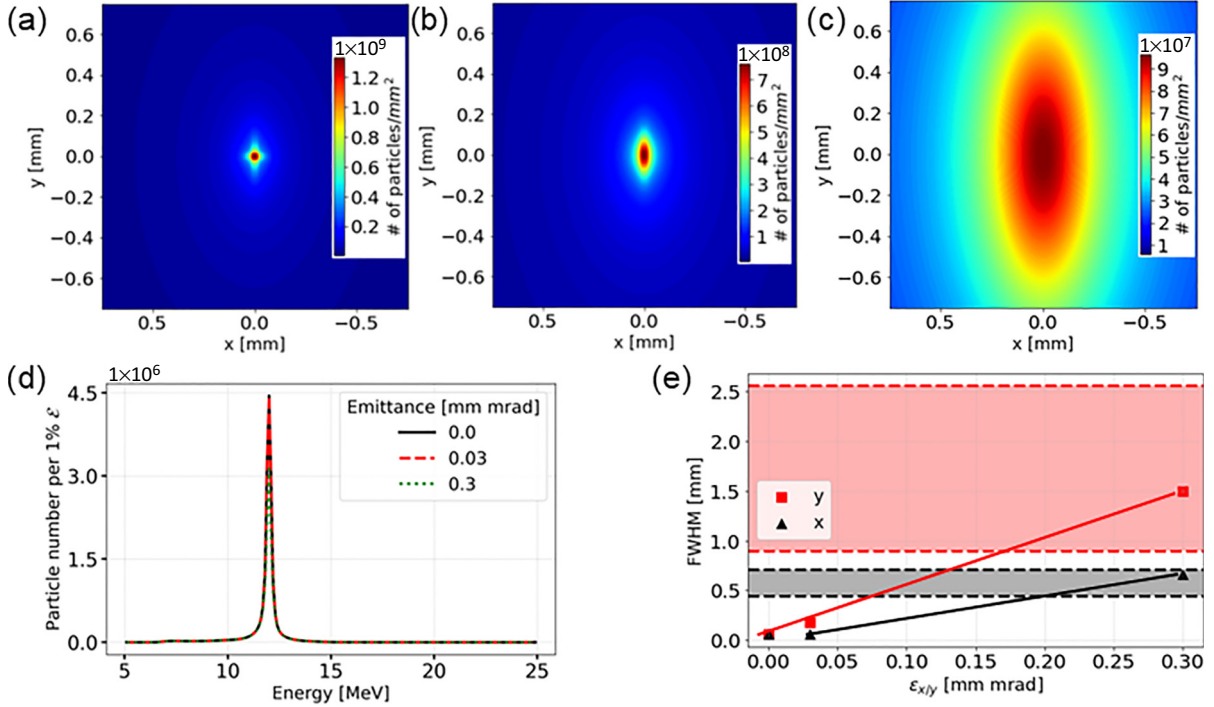


FIG. 3. Calculated proton fluence for 12 MeV with geometrical emittance 0 (a), 0.03 (b), and 0.3 mm mrad (c). (d) Calculated proton spectra that would be expected behind an aperture with 1 mm diameter placed in the proton focus for the three cases (a)–(c). (e) Calculated FWHM (a)–(c) and measured spot size margins (shaded area).

with much smaller emittance. The observations hence suggest that the source properties in this experiment indeed differ strongly from TNSA and hint at a process that increases the spread of the transverse momentum distribution of the protons during or after their acceleration. Instead, it is more likely that the acceleration is governed by induced transparency. It is suggested by the observation that the highest proton energies are observed with 0.1% laser transmission. Various experiments have shown that in such cases, the profile of the accelerated ion bunch is irregular [14,19–21]. The profiles show that trajectories cross in the bunch which corresponds to a degraded emittance compared to the TNSA case. It was explained elsewhere that the transverse temperature is likely very low and that binary Coulomb collisions between charged particles are not the main contributor to the finite emittance [22], because the protons originate from the nonirradiated side of the target and collisions with the very energetic (MeV) electrons are ineffective.

In our case, the target thickness was either 400 or 600 nm, and it seems not adequate attributing the proton source decoupled from the primary laser-plasma interaction at the laser-irradiated side as in TNSA. In particular, the laser field penetrates the plasma with much higher strength than was the case for very thick targets in TNSA. Given the typical laser energy transmission of order 10^{-3} , the plasma electrons and ions are exposed to laser radiation of intensities as high as 10^{18} W/cm² during the laser-plasma interaction and particle acceleration process. Considering, for the sake of the argument, the nonrelativistic equation of motion, a field with normalized vector potential amplitude a_L will drive a particle with charge Qe and mass Mm_n to velocities (normalized to the speed of light) of order $v/c = Q/M \times m_e/m_n \times a_L$. Electrons will move faster than ions by approximately the

ratio of nucleon and electron mass, m_n/m_e . The characteristic time between two collisions with deflection angle of 90° [23] between two unlike particles 1 and 2 can be written as

$$\tau_{12} = \frac{a_L^3}{8\pi r_e^2 c n_2 \ln \Lambda} \frac{1}{q_{12}},$$

where $r_e = 2.82$ fm is the classical electron radius, n_2 is the number density of particle 2, in our case the protons, and $\ln \Lambda \approx \frac{1}{\chi_m}$ is the Coulomb-Logarithm with minimal deflection angle χ_m [24]. The quantity $q_{12} = m_n/m_e Q_1^2 Q_2^2 (M_1 + M_2)^2 M_1 M_2 / |Q_1 M_2 - Q_2 M_1|^3$ collects the charge and mass numbers of the colliding particles; of particular interest are collisions between protons ($Q_2 = 1, M_2 = 1$) and electrons ($Q_1 = -1, M_1 = 1/1836$) or carbon ions ($Q_1 = 6, M_1 = 12$). Collisions of protons with carbons ($q_{CP} \approx 1836 \times 2 \times 12^2$) are considerably more frequent than collisions with electrons ($q_{ep} \approx 1$). A conservative estimate with $a_L \lesssim 1$ and $n_2 \ln \Lambda \gtrsim 10^{21}$ cm⁻³ results in $\tau_{CP} \lesssim 30$ fs; that is, the characteristic collision time is of order of the laser pulse duration.

IV. SIMULATION OF COLLISION EFFECTS

A. Simulation setup

To elucidate this picture more quantitatively, we performed two-dimensional particle-in-cell simulations with the EPOCH code¹ [25]. The simulation box stretched from -10 to $120 \mu\text{m}$

¹Epoch block for the input file; begin:collisions, use_collisions = T, use_nambu = T, coulomb_log = auto, collide = all, coll_n_step = 5, end:collisions.

in the laser propagation direction and from -60 to $+60 \mu\text{m}$ in the transverse direction with resolution of 10 nm . The left boundary at $x = -10 \mu\text{m}$ radiated the laser pulse with a central wavelength of 800 nm and a linear polarization in the y direction. The temporal and spatial distribution of the pulse intensity was Gaussian with FWHM duration of 28 fs and FWHM diameter $4.3 \mu\text{m}$ in the focal plane. At the target position $x = 0$, the peak intensity of $4.3 \times 10^{20} \text{ W/cm}^2$ in focus was reached 1000 fs into the simulation. We refer to this time as $t = 0$. The simulation run time was 2000 fs . The large simulation time after the pulse was necessary to allow the phase space evolution of the protons to settle. We have also performed simulations with non-Gaussian pulse shapes extracted from pulse shape measurements and those required the rather long period of 1000 fs before the peak of the pulse. The evaluation of these runs did not provide added value for understanding the emittance growth and are therefore not shown, but they explain the seemingly unreasonably long simulation time before the peak of the laser pulse.

The remaining three boundaries allow particles and radiation to leave the simulation box. The target was composed of electrons and equal number of protons and fully ionized carbon ions (C^{6+}) to resemble a plastic foil with initial mass density 1 g/cm^3 and thickness 400 nm . The total number of macro particles was 1.56×10^9 . The initial temperature was 10 eV for electrons and 0 for protons and carbon ions. Simulations were performed without and with the binary Coulomb collision model. EPOCH simulates Coulomb collisions using a model combining the works of Nanbu [26] and Perez *et al.* [27]. The number of binary particle-particle collisions is estimated for each simulated particle over a given time period, and a total scatter angle is sampled using the results of numerical simulations. As there is no constraint which requires the collision time period to match the simulation time step, EPOCH can supercycle the collision calculation to improve performance. In the simulations performed in this paper, the collision calculation was performed on every fifth step, using a collision period of five time steps. We chose the automated estimate of the Coulomb logarithm by EPOCH, which relies on local temperature and density estimates.

B. Simulation results

Figure 4 shows the temporal evolution of the emittance of protons for four cases. We generated trace space distributions $f(x, x')$ of accelerated protons on the target rear side every 200 fs , in particular of protons propagating with half divergence angle $< 12^\circ$ in the direction of the laser and with kinetic energies between 11 and 13 MeV . The emittance was calculated via Eq. (1) with the bunch width, divergence, and correlation obtained from integrating over the phase space. When the binary collision model was turned off, the emittance remained low at values between 0.03 and 0.05 mm mrad (red dash-dotted curve). The simulation with collisions between all particles results in a strong growth of the emittance to values of well above 0.3 mm mrad and within the margins of our experimental results. When we deactivate carbon collisions with other species, the emittance saturates at intermediate values around 0.1 mm mrad . Considering binary collisions and changing laser polarization to vertical with respect to the

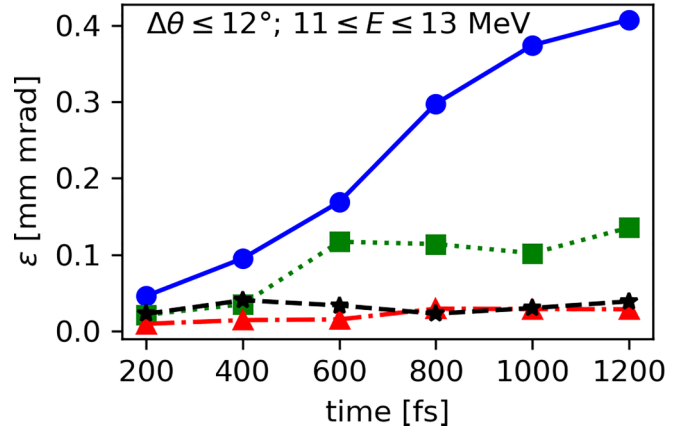


FIG. 4. Temporal evolution of the geometric emittance of protons with energies between 11 and 13 MeV as observed in 2D PIC simulations, without binary Coulomb collisions (red dash-dotted), Coulomb collisions between all particles with p polarization (blue solid), collisions with carbon ions deactivated (green dotted), and laser s polarization vertical to the simulation plane (black dashed). In all cases field ionization is activated.

simulation plane (black dashed curve) the emittance increasing effect vanishes. It shows that when considering collisions, the oscillation of the particles in the laser field contributed to the significant (relative) momentum increase between particles. The emittance growth becomes visible only after the peak of laser-plasma interaction and continues over hundreds of fs. This comparably long period is not representative for when the collisions occur, but rather resembles the time it takes to populate the kinetic energy range 11 – 13 MeV with protons.

V. CONCLUSION

We conclude with two important findings. First, the minimum possible focus size is limited by the intrinsically broad energy spectrum of laser-accelerated proton bunches. Even for a zero emittance source, our beamline geometry would limit minimum focal spot sizes to $60 \mu\text{m}$. This imposes no fundamental limit though; further reduction of the focus size could be achieved for example by including more quadrupole magnets. Second, and, given prior work, somewhat surprising, the proton bunches from plastic foils with 400 and 600 nm thickness exhibit significantly increased transverse emittance compared to TNSA protons from μm thick targets. There have been indications that low- Z materials like plastic might result in increased emittance even for thick targets [28], but binary collisions had not been held responsible for this emittance growth [22]. Our results provide a hint that binary collisions might play a decisive role, in particular for thin targets that transmit significant amounts of laser energy. Although these results do not allow predictions about bunch properties at much higher energies, they indicate that emittance measurements should be considered for acceleration regimes that rely on mechanisms beyond TNSA. According to our very simplistic formula the characteristic time between collisions scales with the transmitted a_L^3 . This means if the intensity increases in order to accelerate protons to higher energies collisions

become less frequent. Therefore one could even expect a smaller effect on emittance as the energy increases and hence smaller proton foci. In any case proton focal spots on the order of 1 mm are already very useful for example for small animal irradiation studies ([29] and references therein). If smaller proton foci are required, for example in minibeam irradiation [30,31], a second focusing element could be added.

ACKNOWLEDGMENTS

We acknowledge support by the Centre for Advanced Laser Applications, T.R. was partially supported by the German

Academic Scholarship Foundation. M.A. acknowledges support from the Leibniz Supercomputing Centre (LRZ) under Application No. 24836. S.M. acknowledges support from Plasma-HEC Consortium EPSRC Grant No. EP/R029148/1 and Archer2 Grant No. ARCHER2-eCSE01-14. S.G. acknowledges financial support from the German Research Foundation (DFG) within the Research Training Group GRK 2274. L.D. acknowledges the support of the DFG within Project No. FOR 2783/1 and F.B. the support of the Bundesministerium für Bildung und Forschung (BMBF) within Project No. 05P18WMFA1. A.P. acknowledges support by the BMBF within Project No. 05P21WMFA1 and the Konrad-Adenauer-Stiftung.

-
- [1] P. R. Bolton, K. Parodi, and J. Schreiber, *Applications of Laser-driven Particle Acceleration* (CRC, Taylor & Francis, Boca Raton, 2018).
- [2] S. C. Wilks, A. B. Langdon, T. E. Cowan, M. Roth, M. Singh, S. Hatchett, M. H. Key, D. Pennington, A. MacKinnon, and R. A. Snavely, *Phys. Plasmas* **8**, 542 (2001).
- [3] E. L. Clark, K. Krushelnick, M. Zepf, F. N. Beg, M. Tatarakis, A. Machacek, M. I. K. Santala, I. Watts, P. A. Norreys, and A. E. Dangor, *Phys. Rev. Lett.* **85**, 1654 (2000).
- [4] H. Wiedemann, *Particle Accelerator Physics* (Springer, Cham, 2015).
- [5] T. E. Cowan, J. Fuchs, H. Ruhl, A. Kemp, P. Audebert, M. Roth, R. Stephens, I. Barton, A. Blazevic, E. Brambrink *et al.*, *Phys. Rev. Lett.* **92**, 204801 (2004).
- [6] M. Borghesi, A. J. Mackinnon, D. H. Campbell, D. G. Hicks, S. Kar, P. K. Patel, D. Price, L. Romagnani, A. Schiavi, and O. Willi, *Phys. Rev. Lett.* **92**, 055003 (2004).
- [7] J. Fuchs, P. Antici, E. dHumires, E. Lefebvre, M. Borghesi, E. Brambrink, C. A. Cecchetti, M. Kaluza, V. Malka, M. Manclossi *et al.*, *Nat. Phys.* **2**, 48 (2005).
- [8] T. Kluge, T. Cowan, A. Debus, U. Schramm, K. Zeil, and M. Bussmann, *Phys. Rev. Lett.* **107**, 205003 (2011).
- [9] K. Zeil, S. D. Kraft, S. Bock, M. Bussmann, T. E. Cowan, T. Kluge, J. Metzkes, T. Richter, R. Sauerbrey, and U. Schramm, *New J. Phys.* **12**, 045015 (2010).
- [10] A. Higginson *et al.*, *Nat. Commun.* **9**, 724 (2018).
- [11] F. Wagner *et al.*, *Phys. Rev. Lett.* **116**, 205002 (2016).
- [12] A. Henig, D. Kiefer, K. Markey, D. C. Gautier, K. A. Flippo, S. Letzring, R. P. Johnson, T. Shimada, L. Yin, B. J. Albright *et al.*, *Phys. Rev. Lett.* **103**, 045002 (2009).
- [13] S. Kar, K. F. Kakolee, B. Qiao, A. Macchi, M. Cerchez, D. Doria, M. Geissler, P. McKenna, D. Neely, J. Osterholz *et al.*, *Phys. Rev. Lett.* **109**, 185006 (2012).
- [14] N. P. Dover *et al.*, *Light Sci. Appl.* **12**, 71 (2023).
- [15] S. Palaniyappan *et al.*, *Nat. Phys.* **8**, 763 (2012).
- [16] L. Obst-Huebl *et al.*, *Nat. Commun.* **9**, 5292 (2018).
- [17] K. Halbach, *Nucl. Instrum. Methods* **169**, 1 (1980).
- [18] T. Rösch *et al.*, *Optimization of a Permanent Magnet Quadrupole Doublet for Laser-Accelerated Proton Bunches at the Centre for Advanced Laser Applications*, SPIE Optics + Optoelectronics Vol. 11779 (SPIE, 2021).
- [19] P. L. Poole *et al.*, *New J. Phys.* **20**, 013019 (2018).
- [20] B. Gonzalez-Izquierdo *et al.*, *Nat. Commun.* **7**, 12891 (2016).
- [21] O. McCusker *et al.*, *Plasma Phys. Controll. Fusion* **65**, 015005 (2023).
- [22] A. J. Kemp, J. Fuchs, Y. Sentoku, V. Sotnikov, M. Bakeman, P. Antici, and T. E. Cowan, *Phys. Rev. E* **75**, 056401 (2007).
- [23] W. L. Kruer, *The Physics of Laser Plasma Interactions* (CRC, Taylor & Francis, Boca Raton, 2018).
- [24] L. D. Landau and E. M. Lifshitz, *Physical Kinetics*, Course of Theoretical Physics (Pergamon Press Ltd., England, 1981), Vol. 10.
- [25] T. D. Arber *et al.*, *Plasma Phys. Controll. Fusion* **57**, 113001 (2015).
- [26] K. Nanbu, *Phys. Rev. E* **55**, 4642 (1997).
- [27] F. Pérez, L. Gremillet, A. Decoster, M. Drouin, and E. Lefebvre, *Phys. Plasmas* **19**, 083104 (2012).
- [28] J. Fuchs, T. E. Cowan, P. Audebert, H. Ruhl, L. Gremillet, A. Kemp, M. Allen, A. Blazevic, J.-C. Gauthier, M. Geissler *et al.*, *Phys. Rev. Lett.* **91**, 255002 (2003).
- [29] K. Parodi *et al.*, *Acta Oncol.* **58**, 1470 (2019).
- [30] S. Girst *et al.*, *Int. J. Radiat. Oncol. Biol. Phys.* **95**, 234 (2016).
- [31] O. Zlobinskaya *et al.*, *Radiat. Environ. Biophys.* **52**, 123 (2013).